Cement and Concrete Research 39 (2009) 966–972

Contents lists available at ScienceDirect

Cement and Concrete Research

journal homepage: http://ees.elsevier.com/CEMCON/default.asp

Fracture of concrete structure using simplified meshless method

Y. Dong *, S. Wu, S.S. Xu, Y. Zhang, S. Fang

Beijing University of Technology, Department of Engineering Mechanics

ARTICLE INFO

Article history:
Received 6 August 2008
Accepted 11 June 2009

Keywords:
Computational mechanics
Crack
Fracture
Meshless
EFG
Material failure
Concrete
Enrichment
Partition of unity

ABSTRACT

Numerical analysis of fracture in concrete is studied with a simplified meshless method. In this meshless method, the crack is represented by a set of disconnected cohesive crack segments that are required to pass through meshless nodes. The crack method therefore falls in the category of discrete crack methods. However, in contrast to most other methods where the crack is represented as continuous line/surface, no representation of the crack surface is needed. Hence, there is no need to track the crack path. Branching cracks and coalescing cracks are a natural outcome of the analysis and no specific algorithms need to be incorporated to model such complicated events. Besides the simplicity of the method, the accuracy is maintained. This is demonstrated through several examples.

© 2009 Elsevier Ltd. All rights reserved.

1. Introduction

The fracture process of structures made of quasi-brittle materials such as concrete is characterized by the formation of microcracks that eventually coalesce and lead to the formation of continuous macro-cracks. Crack propagation in concrete materials is associated with localization of the strain field, which, in case of fully open macrocracks becomes singular across the crack. Obviously, numerical analyses of this class of problems require robust models which adequately represent the discontinuous character of the fracture process. For the modeling of the nonlinear material behavior in the vicinity of the crack tip cohesive crack models [1–7], which take into account a gradual transition from full material strength to zero material strength, are generally adopted.

Since the mid of the 1960s considerable progress has been made in developing models to describe the evolution of cohesive cracks in quasi-brittle materials using continuum-based approaches such as plasticity or damage formulations, rotating or fixed crack models, which, since the mid of the 1980s, have been enhanced by means of adequate regularization techniques (see, e.g. [8,9] for a smeared representations of cracks). At the same time, models allowing for a discrete representation of cracks have been developed by introducing cracks as separate entities directly into the discretization. Meshless methods have become popular for these applications since thanks to the absence of a mesh, discrete cracks can easily be inserted into the discretization [10–22]. Though these methods can handle arbitrary crack propagation, they are usually restricted to a few number of cracks due to computational efficiency. One major difficulty of discrete crack models is representation and cracking of crack surface that becomes cumbersome when number of cracks increase. However, concrete structures generally undergo excessive cracking before failure. Therefore, numerical methods are needed that can handle many cracks.

[23] proposed a method that does not require the crack surface to be continuous and nevertheless gave promising results for dynamic fracture [24]. Their method is based on corrected SPH (Smooth Particle Hydrodynamics) and employsstress-point integration to ensure the stability of the method. The method was extended to three dimensions [25], mode II and mixed mode fracture [26–29] and thin shells [30].

We propose a method based on an idea developed in [23] that can handle many cracks and simultaneously maintain the accurate character of discrete crack models. In contrast to the cracking particles method in [23], our meshless method is based on a local partition of unity where the crack is modeled by discrete crack segments through a node. The method is embedded in a Galerkin method and Gauss quadrature over a background mesh ensures the stability of the method. Such methods areurgently needed to model and understand cracking phenomena in concrete materials. Therefore, there is no need for tracking the crack path. Merging and branching cracks are a natural

* Corresponding author.
E-mail address: ydong@windowslive.com (Y. Dong).

0008-8846/$ – see front matter © 2009 Elsevier Ltd. All rights reserved.
doi:10.1016/j.cemconres.2009.06.014

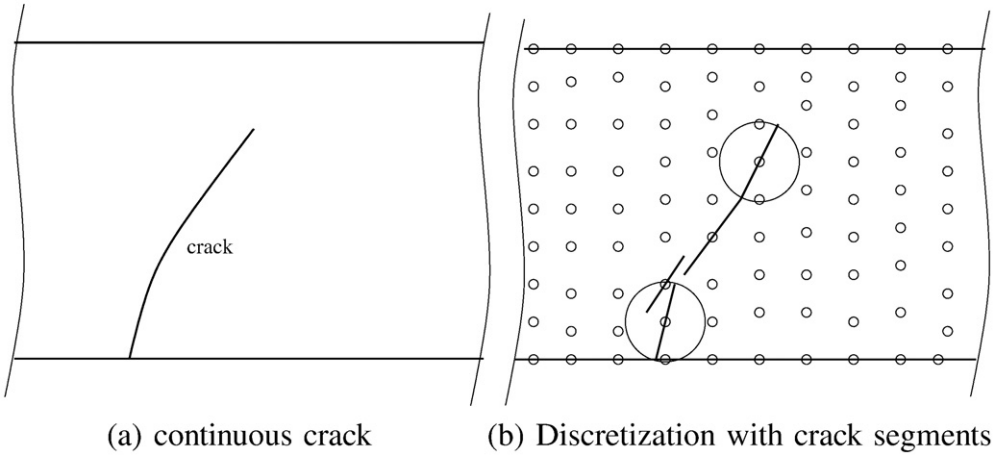

Fig. 1. a) Continuous crack and b) representation of the crack with discrete cohesive crack segments.

outcome of the analysis. This makes the method well suited for simulation of many cracks as they occur in concrete materials.

2. Element free Galerkin method

The elementfree Galerkin (EFG) method [31] is derived from Moving-least-squares (MLS) approximation, that can be written in terms of a polynomial basis $\mathbf{p}(\mathbf{x})$ and unknown coefficients $\mathbf{a}(\mathbf{x})$:

$$\mathbf{u}^{\mathrm{con}}(\mathbf{x}) = \sum_{\mathrm{I}=1}^{\mathrm{NP}} \mathrm{p}_{\mathrm{I}}(\mathbf{x})\mathrm{a}_{\mathrm{I}}(\mathbf{x}) \tag{1}$$

Here, the superimposed *con* denotes the *continuous* character of the approximation, $\mathbf{p}$ is set to $\mathbf{p}^T(\mathbf{x}) = (1, x, y)$ and hence $NP = 3$.

Let us define the discrete weighted $\mathcal{L}_2$ error norm J

$$J = \sum_{I=1}^{N} \left(\mathbf{P}^{\mathrm{T}}(\mathbf{x}_{\mathrm{I}})\mathbf{a}(\mathbf{x}_{\mathrm{I}}) - \mathbf{u}_{\mathrm{I}}\right)^2 \mathrm{w}(\mathbf{x} - \mathbf{x}_{\mathrm{I}}, \mathrm{h}) \tag{2}$$

with kernel function $w(\mathbf{x}-\mathbf{x}_I, h)$ where h is the interpolation radius of the kernel function, $\mathbf{P}^T(\mathbf{x}_I)$ $\mathbf{a}(\mathbf{x}_I)$ is the matrix expression of Eq. (1) and N is the number of nodes that are within this interpolation radius. The number of nodes N has to be larger (or at least equal) than the number of polynomial functions NP in order to uniquely determine the unknown coefficients $\mathbf{a}$. We chose the quartic B-spline with circular support size for our kernel function:

$$w(\mathbf{x} - \mathbf{x}_{\mathrm{I}}, \mathrm{h}) = \mathrm{w}(\mathrm{s}) = \begin{cases} 1 - 6\mathrm{s}^2 + 8\mathrm{s}^3 - 3\mathrm{s}^4 & \mathrm{s} \le 1 \\ 0 & \mathrm{s} > 1 \end{cases} \tag{3}$$

with $s = \mathbf{x}\frac{\mathbf{x}_{\mathrm{I}}}{2\mathrm{h}}$ for circular support size. The size $2h$ is the interpolation radius and is 2 times the distance between nodes in accordance with e.g. [32,33].

Minimizing J, Eq. (2), with respect to the unknown coefficients $\mathbf{a}$ leads to the final EFG approximation

$$\mathbf{u}^{\mathrm{con}}(\mathbf{x}) = \sum_{\mathrm{I}=1}^{\mathrm{N}} \mathbf{N}_{\mathrm{I}}(\mathbf{x})\mathbf{u}_{\mathrm{I}} \tag{4}$$

with the meshless shape functions

$$N_I(\mathbf{x}) = \mathbf{p}^{\mathrm{T}}(\mathbf{x})\mathbf{A}^{-1}(\mathbf{x})\mathbf{D}_{\mathrm{I}}(\mathbf{x}) \tag{5}$$

and

$$\begin{aligned} \mathbf{D}_I(\mathbf{x}) &= w(\mathbf{x}-\mathbf{x}_I, h)\mathbf{p}^T(\mathbf{x}_I) \\ \mathbf{A}_I(\mathbf{x}) &= \sum_I w(\mathbf{x}-\mathbf{x}_I, h)\mathbf{p}(\mathbf{x}_{\mathrm{I}})\mathbf{p}^{\mathrm{T}}(\mathbf{x}_{\mathrm{I}}) \end{aligned} \tag{6}$$

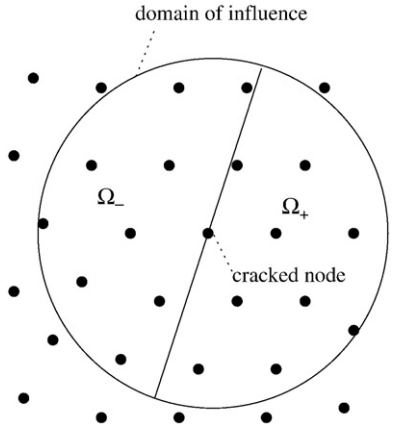

Fig. 2. Cracked node where the crack segment crosses the entire domain of influence of the node.

3. Displacement field approximation

Crack is a discontinuity in the displacement field. Therefore, Eq. (5) is complemented with another term that is capable to capture the jump in the displacement field. We can think of decomposing the displacement field into a continuous part $\mathbf{u}^{con}$, Eq. (5), and discontinuous part $\mathbf{u}^{dis}$ that will be defined subsequently:

$$\mathbf{u}(\mathbf{x}) = \mathbf{u}^{\mathrm{con}}(\mathbf{x}) + \mathbf{u}^{\mathrm{dis}}(\mathbf{x}) \tag{7}$$

To discretize the discontinuous displacement field, we take advantage of the local partition of unity [34] method, local means that the approximation is only modified in the vicinity of the crack. The partition of unity concept is especially useful in the context of material failure since the kinematics of the crack can be incorporated into the formulation elegantly.

Instead of describing the crack as continuous surface, we propose to model the discrete crack by a set of cohesive crack segments that

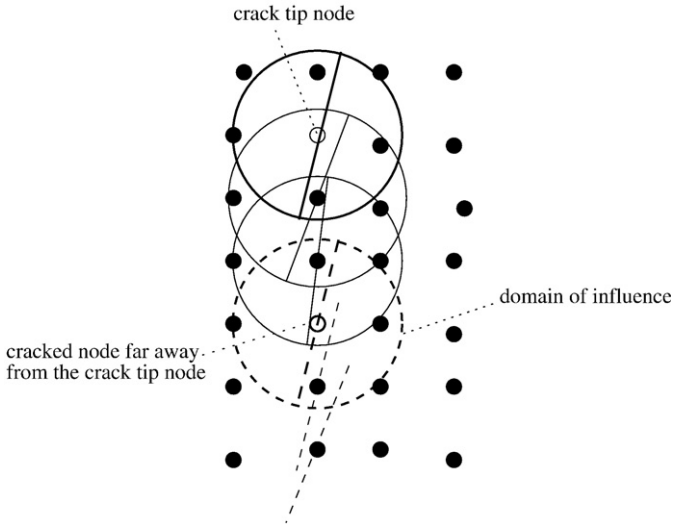

Fig. 3. Fixed crack segments illustrated by dashed lines for nodes far away from the crack segment of the node at the tip. Rotated crack segments are illustrated by solid lines.

pass through the entire domain of influence of a node, Fig. 1. This circumvents the need of tracking the crack path. There is no need for specific algorithms that treat branching and merging cracks which is a natural outcome of the analysis. This makes the method very robust and applicable to problems with many cracks.

The jump in the displacement field is obtained by the discontinuous displacement approximation that is active only for nodes that contain the cohesive crack segments:

$$\mathbf{u}^{dis}(\mathbf{x}) = \sum_{I\in[??]_c} N_I(\mathbf{x})\Psi(\mathbf{x})\mathbf{q}_I \tag{8}$$

where $[??]_c$ are the nodes where the cohesive crack segments pass through, $\mathbf{q}_I$ are additional unknowns and $\Psi(\mathbf{x})$ is the enrichment function:

$$\Psi(\mathbf{x}) = \begin{cases} 1 & \text{if}\mathbf{n}\cdot(\mathbf{x}-\mathbf{x}_I) > 0(10) \\ -1 & \text{if}\mathbf{n}\cdot(\mathbf{x}-\mathbf{x}_I) < 0(11) \end{cases} \tag{9}$$

Note that only cracked nodes are enriched. The length of the cohesive segment is equal to the size of the domain of influence of the associated cracked node. The jump in the displacement field $[[\mathbf{u}]] = \mathbf{u}^{\Omega+} - \mathbf{u}^{\Omega-}$, where the subscript of Ω indicates the different sides of the crack, Fig. 2, only depends on the additional degrees of freedom $\mathbf{q}_I$:

$$[[\mathbf{u}(\mathbf{x})]] = \sum_{I\in[??]_c} 2N_I(\mathbf{x})\mathbf{q}_I \tag{10}$$

Omega-Ω_- Omega $+\,\Omega_+$.
The discrete strain field can be derived as

$$\nabla\mathbf{u}^s(\mathbf{x}) = \sum_{I\in[??]} \nabla N_I(\mathbf{x})\mathbf{u}_I + \sum_{I\in[??]_c} \nabla N_I(\mathbf{x})\Psi(\mathbf{x})\mathbf{q}_I \tag{11}$$

where $[??]$ is the set of all nodes and $[??]_c$ is the set of cracked nodes.

4. Cracking criterion

We used the Rankine criterion to generate a crack. The crack is introduced once the maximum principal tensile stress exceeds the uni-axial tensile strength. To avoid erratic crack patterns, the stress field in the vicinity of cracked nodes are averaged. The non-local stress tensor P is computed as a weighted average of the stresses at *NG* Gauss

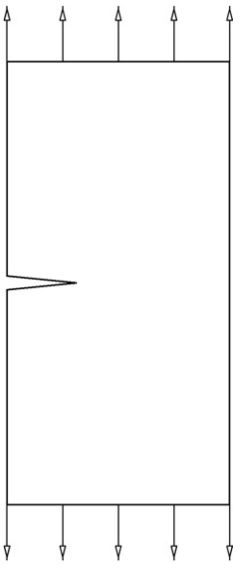

Fig. 4. Plate in tension.

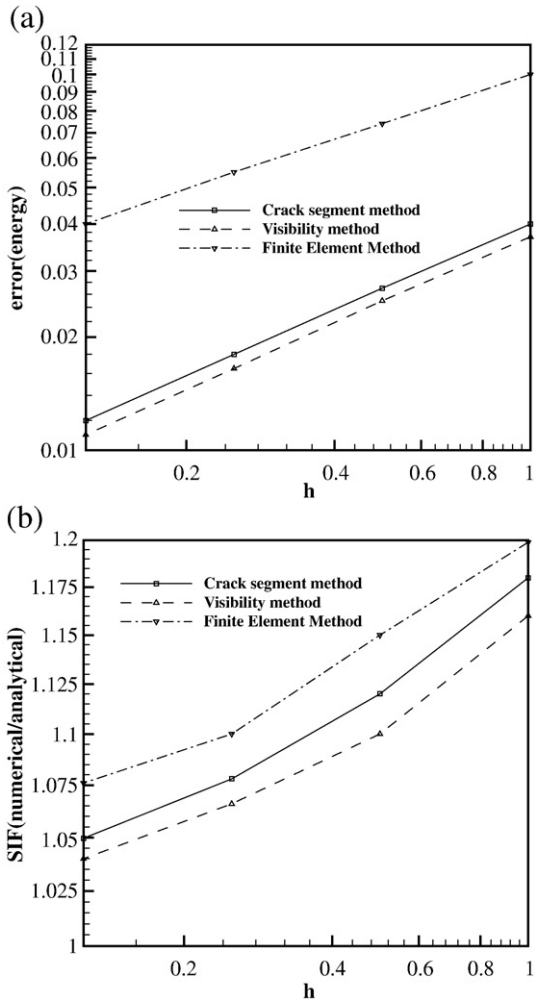

Fig. 5. Results for the plate in tension.

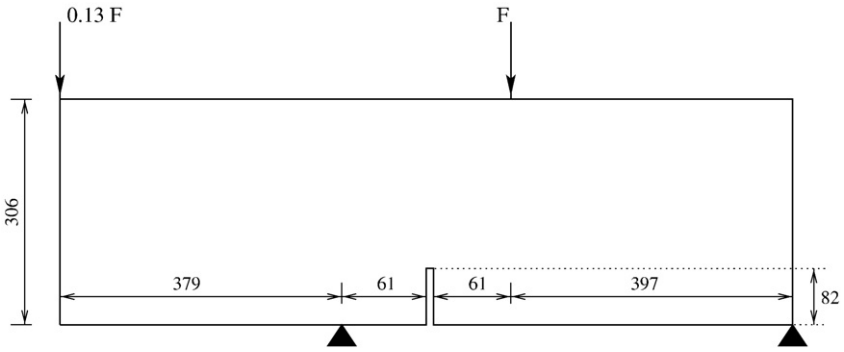

Fig. 6. The pre-notched beam subject to two concentrated loads; all dimensions are in mm.

points. It results from the sum of the local stresses $\mathbf{P}_I$ at the Gauss points I, weighted with $\hat{w}_I$ and the associated area A_I:

$$\overline{\mathbf{P}} = \sum_{I}^{NG} \mathbf{P}_I \hat{w}_I A_I \tag{12}$$

with

$$\hat{w}(s) = \frac{w(s)}{\sum_{I}^{NG} w_I A_I} \tag{13}$$

where $w(s)$ is the quartic B-spline.

The stress field will change when the crack propagates. The Rankine criterion for crack initiation is met when only small changes of the principal (stress) axes occur. Therefore, we allow the crack segments to rotate according to changes of the direction of principal stress axis. This avoids artificial cracking of already existing macro-cracks far away from the crack tip (Fig. 3).

5. The cohesive law

In the cohesive model, the traction is related to the crack opening, Eq. (13):

$$t_n = f_t - \frac{f_t}{\delta_{max}}[[u]]_n \text{if} [[u]]_n < \delta_{max} \text{ and } [[u]]_n^{t+\Delta t} > [[u]]_n^t \quad \text{otherwise} t_n = 0 \text{ when } [[u]]_n^{t+\Delta t} > [[u]]_n^t \tag{14}$$

where

$$[[u]]_n = \mathbf{n} \cdot [[\mathbf{u}]] \tag{15}$$

is the crack opening and δ_{max} is the point where the traction have decayed to zero. Unloading is linear elastic. We neglected shear traction in our studies but intend to incorporate them in the future.

6. Equilibrium equations and discretization

The equation of equilibrium is given by

$$\nabla \cdot \mathbf{P} + \mathbf{b} = 0, \mathbf{x} \in \Omega \tag{16}$$

$$\mathbf{u} = \mathbf{u}, \mathbf{x} \in \Gamma_u \tag{17}$$

$$\mathbf{n}_t \cdot \mathbf{P} = \mathbf{t}, \mathbf{x} \in \Gamma_t \tag{18}$$

$$\mathbf{n}_c \cdot \mathbf{P} = \mathbf{t}_c([[\mathbf{u}]]), \mathbf{x} \in \Gamma_c \tag{19}$$

where $\mathbf{u}$ are the displacements, $\mathbf{t}$ are the tractions, $\mathbf{P}$ is the stress tensor, $\mathbf{b}$ are the body forces, Γ is the boundary and the subscript u, t, c denote "displacement", "traction" and "crack", respectively. With the test functions $\mathbf{v}$ that are of similar structure than the trial functions, Eqs. (5) and (9), the weak form of the equations of equilibrium can be assembled:

$$\sum_{j=1}^{n} \left[\int_{\Omega_j} \nabla^s \mathbf{v}_j : \mathbf{P} d\Omega + \int_{\Gamma_{cj}} \mathbf{v} \cdot \mathbf{t}_c d\Gamma \right] = \sum_{j=1}^{n} \int_{\Gamma_{tj}} \mathbf{v} \cdot \mathbf{t} d\Gamma \tag{20}$$

Inserting the trial functions, Eqs. (9) and (5), and the test functions that are of similar structure into Eq. (23), the equation to be solved is given in matrix form:

$$\int_\Omega \hat{\mathbf{B}}^T \mathbf{P} d\Omega + \int_{\Gamma_c} \hat{\mathbf{N}}^T \mathbf{t}_c d\Gamma = \int_{\Gamma_t} \hat{\mathbf{N}}^T \mathbf{t} d\Gamma + \int_\Omega \hat{\mathbf{N}}^T \mathbf{b} d\Omega \tag{21}$$

where $\hat{\mathbf{B}}$ and $\hat{\mathbf{N}}$ contain continuous and discontinuous shape functions and their spatial derivatives, respectively. Continuous B-matrix:

$$\mathbf{B}_I^u = \begin{bmatrix} N_{I,x} & 0 \\ 0 & N_{I,y} \\ N_{I,y} & N_{I,x} \end{bmatrix} \tag{22}$$

Discontinuous B-matrix:

$$\mathbf{B}_I^q = \begin{bmatrix} \tilde{N}_{I,x} & 0 \\ 0 & \tilde{N}_{I,y} \\ \tilde{N}_{I,y} & \tilde{N}_{I,x} \end{bmatrix} \tag{23}$$

with $\tilde{\mathrm{N}} = N\Psi(\mathbf{x})$.

The final system of equations

$$\begin{bmatrix} \mathbf{K}_{IJ}^{uu} & \mathbf{K}_{IJ}^{uq}(27) \\ \mathbf{K}_{IJ}^{qu} & \mathbf{K}_{IJ}^{qq} \end{bmatrix} \cdot \begin{bmatrix} \Delta \mathbf{u}_J(28) \\ \Delta \mathbf{q}_J \end{bmatrix} = \begin{bmatrix} \mathbf{f}_{I,ext}^u - \mathbf{f}_{I,int}^u(29) \\ \mathbf{f}_{I,ext}^q - \mathbf{f}_{I,int}^q \end{bmatrix} \tag{24}$$

is solved with an incremental iteration scheme in which

$$\mathbf{K}_{IJ}^{ij} = \int_\Omega (\mathbf{B}_I^i)^T \mathbf{C} \mathbf{B}_J^j d\Omega + \kappa \int_{\Gamma_c} \mathbf{N}^T \mathbf{D} \mathbf{N} d\Gamma \tag{25}$$

where $\kappa = 1$ when $i = j = q$, otherwise $\kappa = 0$, $\mathbf{D}$ is the tangential stiffness of the cohesive model and the superscript i and j indicate u and q for the continuous and discontinuous shape functions and

$$\mathbf{f}_{I,ext}^i = \int_{\Gamma_t} (\mathbf{N}_I^i)^T \mathbf{t} d\Gamma + \int_\Omega (\mathbf{N}_I^i)^T \mathbf{b} d\Omega \tag{26}$$

$$\mathbf{f}_{I,int}^i = \int_\Omega (\mathbf{B}_I^i)^T \mathbf{P} d\Omega + \int_{\Gamma_c} (\mathbf{N}_I^q)^T \mathbf{t}_c d\Gamma \tag{26}$$

The integrals are evaluated by Gauss quadrature. Therefore, a background mesh is constructed such that the EFG nodes span the background mesh. More detailed about Gauss quadrature in the EFG method can be found e.g. in [33,35].

7. Stability of the discrete meshless crack method

Meshfree methods suffer sometimes from instability. The instability due to rank deficiency occurs for meshfree methods that deploy nodal position as quadrature points [35]. This instability is similar to the instabilities observed for finite elements using reduced integration. We avoid this instability by using Gauss quadrature. Therefore, a background mesh is constructed. Since the EFG method is based on rational shape functions, Gauss integration is not exact. A higher number of quadrature points reduces integration errors [36] and simultaneously removes the instability due to rank deficiency.

The tensile instability in meshfree methods occurs when the kernel function is expressed in terms of spatial co-ordinates **x**. It results in numerical fracture once tensile stresses occur. This instability is eliminated by the use of Lagrangian kernel function that is expressed in terms of material co-ordinates **X** [35]. The use of Lagranigan kernel function is especially important for modeling fracture as was demonstrated by [35].

8. Results

After validation of our method, we present three examples: The first example is a pre-notched sample under four-point bending. The second example is mixed-mode failure of concrete and the last example is a 3-point bending beam that develops several cracks.

8.1. Validation

To validate our method, we studied examples where an analytical solution is available. We present results for plate under uni-axial tension, Fig. 4. We solved this problem with three different methods:

- Finite element method with bilinear quadrilateral shape functions
- EFG method with visibility criterion
- Crack segment method

In the finite element analysis, the crack is aligned with the crack. In the crack segment method, the crack segments are placed in the middle of the specimen. The error in the energy norm is shown in Fig. 5a. The meshless methods are more accurate than the finite element method. The crack segment method is of the same accuracy as the EFG method with visibility criterion but the crack segment method is computationally more efficient since it does not require representation of crack surface. Fig. 5b shows the stress intensity factor (SIF) K_I for the problem. Visibility method and crack segment method are more accurate than finite element method and the crack segment method is similar to visibility method.

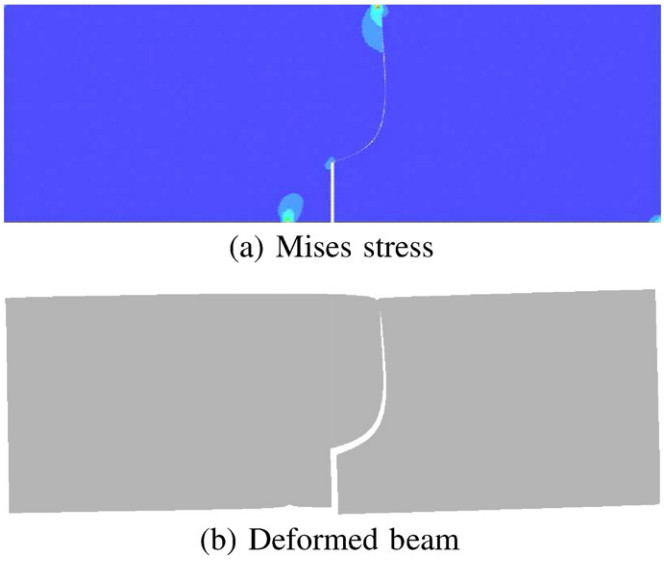

Fig. 7. Crack in the tensile-shear beam.

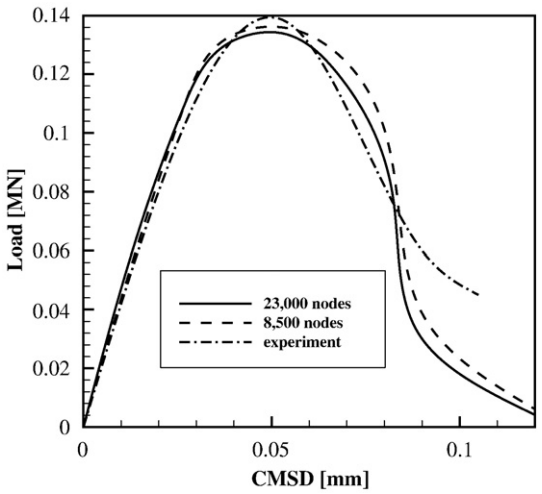

Fig. 8. Load vs. crack mouth sliding displacement.

8.2. Tensile-shear beam

Consider the pre-notched beam in Fig. 6 that is subjected to concentrated forces *F*. Experimental data was reported by [37]. The beam has a rectangular cross-section with thickness 156mm. The pre-notch has a length of 82mm. The material's Young's modulus is $E=25{,}000$MPa, Poisson's ratio $v=0.2$, tensile strength $f_t=2.8$MPa and fracture energy $G_f=100$N/m.

The crack propagates from the pre-notch obliquely. Initially shear stresses dominate the crack orientation. In the later stage, dominant tensile stresses cause the crack to straighten. Fig. 7 shows the crack pattern at the end of the simulation. The load-deflection curve is in close agreement with the load-deflection curve reported in [37] (Fig. 8).

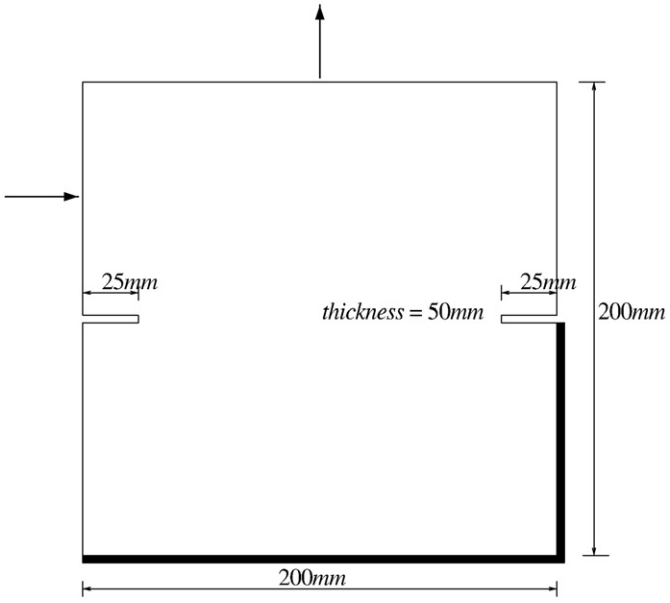

Fig. 9. Nooru-Mohamed mixed-mode test [38].

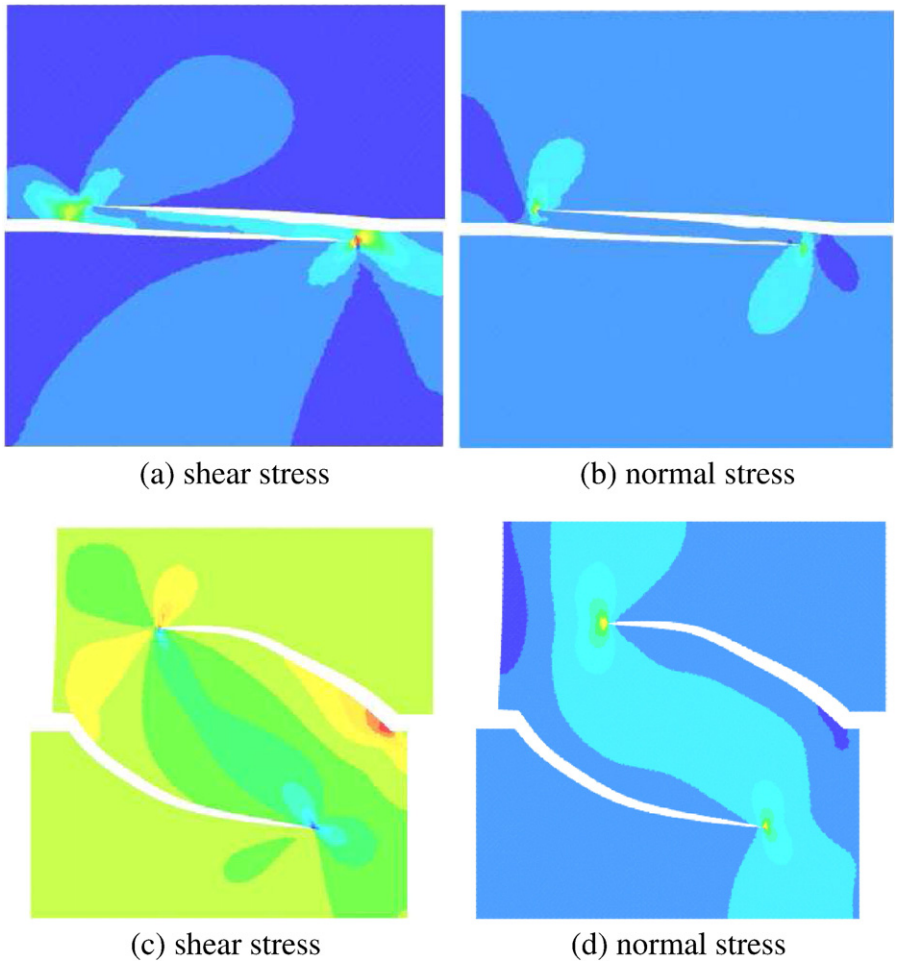

Fig. 10. Results for the Nooru-Mohamed test; a),b) for a shear force of 5kN and c),d) for a shear force of 27.38kN.

8.3. Nooru-Mohamed test

Next example is the mixed-mode fracture test of [38]. A double notched specimen as depicted in Fig. 9 is loaded simultaneously in tension and shear. In the experiment, the shear force is first increased up to a certain value while the tensile force is kept zero. Then, the shear force is kept constant while the tensile force is increased until the specimen fails. We consider displacement control experiments with

(1) shear force = 5kN
(2) shear force = 27.38kN

In the first case, the crack paths was almost straight while a curved crack paths occurs for case two. This experiment is often used to test numerical methods.

The crack paths and stress distribution for our numerical simulation is illustrated in Fig. 10. We capture the straight as well as the curved crack paths as they approximately occurred in the experiment. Fig. 11 compares the load displacement curves of simulation and experiment.

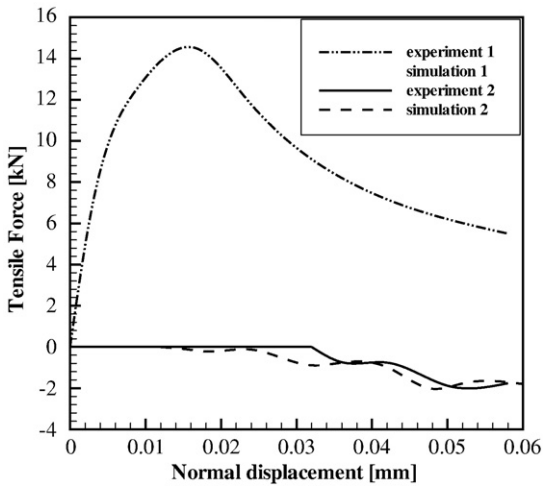

Fig. 11. Tensile Force-normal displacement curve for the Nooru-Mohamed tests.

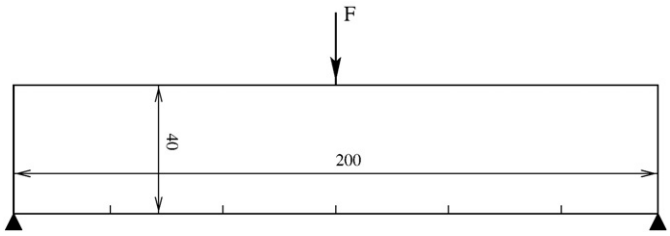

Fig. 12. 3-point beam in bending, all dimensions are in mm.

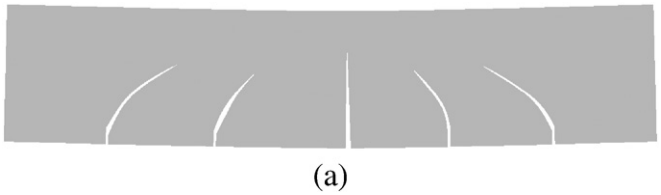

Fig. 13. Cracks in the 3-point bending beam.

8.4. 3-point bending beam

The last example is the 3-point bending beam in bending illustrated in Fig. 12. There are five little vertical imperfections (pre-cracks) of 2mm length in order to facilitate crack propagation.

The material has a Young's modulus $E=36{,}000$MPa, Poisson's ratio $v=0.2$, tensile strength $f_t=3$MPa, $\delta_{max}=0.33$mm and fracture energy $G_f=100$N/m. Initially, bending stresses are dominant at crack initiation at the bottom and cracks propagate perpendicular to the bottom line. The cracks incline due to shear stresses at a later stage. Fig. 13 shows the crack pattern at the end of the simulation. There is no experimental data available but the crack pattern looks reasonable.

9. Conclusions

We studied fracture of concrete structure with a simplified meshless method. Therefore, fracture is modeled with discrete crack model. Modeling of fracture is important for assessment and reliability analysis of concrete structures. Since the global response is influenced by local phenomena such as cracking, a detailed crack model is needed. In our discrete crack method, the crack was modeled by a set of cohesive crack segments that directly pass through the nodes such that no representation of the crack surface is necessary. This makes the method ideally suited for concrete due to occurrence of many cracks in the concrete material. It simultaneously maintains the high accuracy of discrete crack methods.

In the future, we will extend the method to reinforced and fibre reinforced concrete structures with bigger dimensions. These structures undergo excessive cracking. They are currently developed at our Institute and our method will be extended to predict the behavior of these structures.

References

[1] G. Barenblatt, The mathematical theory of equilibrium of cracks in brittle fracture, Advances in Applied Fracture 7 (1962) 55–129.
[2] A. Hillerborg, M. Modeer, P.E. Peterson, Analysis of crack formation and crack growth in concrete by means of fracture mechanics and finite elements, Cement and Concrete Research 6 (1976) 773–782.
[3] M. Ortiz, Y. Leroy, A. Needleman, Finite element method for localized failure analysis, Computer Methods in Applied Mechanics and Engineering 61 (1987) 189–213.
[4] X.-P. Xu, A. Needleman, Numerical simulations of fast crack growth in brittle solids, Journal of the Mechanics and Physics of Solids 42 (1994) 1397–1434.
[5] I. Carol, C.M. Lopez, O. Roa, Micromechanical analysis of quasi-brittle materials using fracture-based interface elements, International Journal for Numerical Methods in Engineering 52 (1996) 193–215.
[6] J.C. Galves, J. Cervenka, D.A. Cendon, V. Saouma, A discrete crack approach to normal/shear cracking of concrete, Cement and Concrete Research 320 (10) (2002) 1567–1585.
[7] K.M. Lee, J.H. Park, A numerical model for elastic modulus of concrete considering interfacial transition zone, Cement and Concrete Research 380 (3) (2008) 396–402.
[8] Z.P. Bazant, B.H. Oh, Crack band theory for fracture in concrete, Materials and Structures 16 (1983) 155–177.
[9] Z.P. Bazant, T. Belytschko, Wave propagation in a strain softening bar: exact solution, Journal of Engineering Mechanics ASCE 11 (1985) 381–389.
[10] R. De Borst, Modern domain-based discretization methods for damage and fractures, International Journal of Fracture 1380 (1-4) (2006) 241–262.
[11] D. Organ, M. Fleming, T. Terry, T. Belytschko, Continuous meshless approximations for nonconvex bodies by diffraction and transparency, Computational Mechanics 18 (1996) 225–235.
[12] T. Belytschko, Y.Y. Lu, L. Gu, Crack propagation by element-free galkerin methods, Engineering Fracture Mechanics 51 (1994) 295–315.
[13] T. Belytschko, Y.Y. Lu, Element-free galerkin methods for static and dynamic fracture, International Journal of Solids and Structures 32 (1995) 2547–2570.
[14] T. Belytschko, Y.Y. Lu, L. Gu, Crack propagation by element-free galerkin methods, Engineering Fracture Mechanics 510 (2) (1995) 295–315.
[15] S. Hao, W.K. Liu, C.T. Chang, Computer implementation of damage models by finite element and meshfree methods, Computer Methods in Applied Mechanics and Engineering 1870 (3-4) (2000) 401–440.
[16] S. Hao, W.K. Liu, D. Qian, Localization-induced band and cohesive model, Journal of Applied Mechanics-Transactions of the ASME 670 (4) (2000) 803–812.
[17] T. Rabczuk, P. Areias, A meshfree thin shell for arbitrary evolving cracks based on an extrinsic basis, Computer Modeling in Engineering & Sciences 160 (2) (2006) 115–130.
[18] T. Rabczuk, G. Zi, A meshfree method based on the local partition of unity for cohesive cracks, Computational Mechanics 390 (6) (2007) 743–760.
[19] G. Zi, T. Rabczuk, W. Wall, Extended meshfree methods without branch enrichment for cohesive cracks, Computational Mechanics 400 (2) (2007) 367–382.
[20] S. Li, BoC. Simonson, Meshfree simulation of ductile crack propagation, International Journal for Computational Methods in Engineering Science and Mechanics 6 (2003) 1–19.
[21] S. Hao, W.K. Liu, P.A. Klein, A.J. Rosakis, Modeling and simulation of intersonic crack growth, International Journal of Solids and Structures 410 (7) (2004) 1773–1799.
[22] S. Hao, W.K. Liu, Moving particle finite element method with superconvergence: Nodal integration formulation and applications, Computer Methods in Applied Mechanics and Engineering 1950 (44-47) (2006) 6059–6072.
[23] T. Rabczuk, T. Belytschko, Cracking particles: A simplified meshfree method for arbitrary evolving cracks, International Journal for Numerical Methods in Engineering 610 (13) (2004) 2316–2343.
[24] T. Rabczuk, J. Eibl, Simulation of high velocity concrete fragmentation using SPH/MLSPH, International Journal for Numerical Methods in Engineering 56 (2003) 1421–1444.
[25] T. Rabczuk, T. Belytschko, A three dimensional large deformation meshfree method for arbitrary evolving cracks, Computer Methods in Applied Mechanics and Engineering 196 (2007) 2777–2799.
[26] T. Rabczuk, T. Belytschko, Application of particle methods to static fracture of reinforced concrete structures, International Journal of Fracture 1370 (1-4) (2006) 19–49.
[27] T. Rabczuk, P.M.A. Areias, A new approach for modelling slip lines in geological materials with cohesive models, International Journal for Numerical and Analytical Methods in Geomechanics 300 (11) (2006) 1159–1172.
[28] T. Rabczuk, P.M.A. Areias, T. Belytschko, A simplified mesh-free method for shear bands with cohesive surfaces, International Journal for Numerical Methods in Engineering 690 (5) (2007) 993–1021.
[29] T. Rabczuk, E. Samaniego, Discontinuous modelling of shear bands using adaptive meshfree methods, Computer Methods in Applied Mechanics and Engineering 197 (2008) 641–658.
[30] T. Rabczuk, P.M.A. Areias, T. Belytschko, A meshfree thin shell method for non-linear dynamic fracture, International Journal for Numerical Methods in Engineering 720 (5) (2007) 524–548.
[31] T. Belytschko, Y.Y. Lu, L. Gu, Element-free galerkin methods, International Journal for Numerical Methods in Engineering 37 (1994) 229–256.
[32] T. Belytschko, Y. Krongauz, D. Organ, M. Fleming, P. Krysl, Meshless methods: An overview and recent developments, Computer Methods in Applied Mechanics and Engineering 139 (1996) 3–47.
[33] J. Dolbow, T. Belytschko, An introduction to programming the meshless element free galerkin method, Archives of Computational Methods in Engineering 50 (3) (1998) 207–241.
[34] J.M. Melenk, I. Babuska, The partition of unity finite element method: Basic theory and applications, Computer Methods in Applied Mechanics and Engineering 139 (1996) 289–314.
[35] T. Rabczuk, T. Belytschko, S.P. Xiao, Stable particle methods based on lagrangian kernels, Computer Methods in Applied Mechanics and Engineering 193 (2004) 1035–1063.
[36] T. Rabczuk, T. Belytschko, Adaptivity for structured meshfree particle methods in 2d and 3d, International Journal for Numerical Methods in Engineering 630 (11) (2005) 1559–1582.
[37] M. Arrea, A.R. Ingraffea, Mixed-mode crack propagation in mortar and concrete, Technical Report 81-13, Department of Structural Engineering, Cornell University New York, 1982.
[38] M.B. Nooru-Mohamed. *Mixed-mode fracture of concrete: an experimental approach*. PhD thesis, Delft University of Technology, PhD-thesis, 1992.